Finite element/boundary element coupling for airbag deployment

IV International Conference on Computational Methods for Coupled Problems in Science and Engineering
COUPLED PROBLEMS 2011
M. Papadrakakis, E. Oñate and B. Schrefler (Eds)

FINITE ELEMENT/BOUNDARY ELEMENT COUPLING FOR AIRBAG DEPLOYMENT

T.M. van Opstal[†,*] and E.H. van Brummelen[†]

[†]Multi-Scale Engineering Fluid Dynamics (MEFD),
Eindhoven, University of Technology,
P.O. Box 513, 5600MB, Netherlands.

*email: t.m.v.opstal@tue.nl, web page: http://w3.tue.nl

Key words: Fluid–structure interaction, boundary element method, strong coupling, dynamic

Abstract. Fluid–structure interaction of inflatables comprizes a family of applications, of which airbags are one. Challenges in this domain are complex geometries requiring relatively high resolution; large displacements possibly entailing severe mesh distortion; and strong coupling. A promising approach seems to be coupling a classical finite element formulation for the airbag fabric to a boundary element formulation for the enclosed fluid. Together with an appropriate time-integration scheme this method answers aforementioned challenges, as demonstrated by numerical simulation.

1 Introduction

In a small percentage of airbag deployments, out-of-position impact occurs, usually resulting in severe injuries. To understand and improve the inflation process, a precise understanding of the airbag dynamics is required. This can be provided by accurate numerical simulations. These simulations are a complicated endeavor however, mainly on account of the large displacements and length-scale disparities inherently involved. On the one hand, a realistic stowed airbag constitutes a labyrinth of intricate folds. On the other, the final configuration is a relatively simple bulb. To date, the complex behavior on the small scales has been overly simplified (e.g. [9]) rendering the results inappropriate for the analysis of out-of-position situations.

The approach proposed here is to decompose the fluid domain according to the above-mentioned length-scales. The flow inside the geometrically complex folded region is described by a simple, linear potential flow model. This enables analysis using the boundary element method (BEM), which offers significant advantages over domain-discretization approaches. Most prominently: the anticipated large displacements do not entail mesh

skewing problems; the solution is calculated exclusively at the coupling interface; and the structure mesh can be inherited by the fluid.

To assess the aforementioned approach, we consider a fluid-structure-interaction problem consisting of a potential-flow model coupled to a string model described by a nonlinear wave equation. The latter is discretized with the finite element method. The system requires the imposition of volume conservation on the structure subproblem to account for the incompressibility of the fluid, and setting of an arbitrary additive constant on the fluid solution, both by means of a Lagrange multiplier. Also, due to the typically low mass of the membrane and the incompressibility of the fluid, the added-mass effect [2, 3, 5] requires the use of an implicit time-integration scheme.

The remainder of this paper is organized as follows. In sec. 2, the mathematical problem is introduced. From the governing equations suitable variational forms are derived. Some properties pertaining to the numerical solution of the system are elucidated. In sec. 3, the discretization in both space and time of the variational forms is treated. Ensuing, sec. 4 presents numerical verification and demonstration of the proposed method. This leads to the conclusions, which are drawn in sec. 5.

2 Problem statement

The structure is assumed to behave according to a large-displacement string model. The fluid is assumed inviscid and irrotational. In this section variational forms for the structural and fluidic subsystems are given, followed by their coupling and a discussion on the aggregate system.

Membrane The airbag, henceforth designated the membrane, is modeled by a curve in the plane parametrized by $\boldsymbol{x} : (0, L)\times(0, T) \longrightarrow \mathbb{R}^2$. This membrane is defined by the time dependent set $\Gamma_w := \boldsymbol{x}((0, L), t)$. Together with the inflater opening Γ_i, it encloses the fluid domain Ω, which is consequently also time dependent. The boundary $\Gamma := \overline{\Gamma_w \bigcup \Gamma_i}$ is assumed to be $C^{1,1}$-continuous almost everywhere. Time- and space derivatives are denoted $\partial_t(\cdot)$ and $\partial_s(\cdot)$, respectively. The motion of the membrane is governed by the momentum-balance equation [1, 13]:

$$\varrho_0 \partial_t^2 \boldsymbol{x} - \partial_s \left(E[1 - J^{-1}]\partial_s \boldsymbol{x} \right) - Jp\boldsymbol{n} = 0, \tag{1}$$

supplemented with initial conditions $\boldsymbol{x}(\cdot, 0) = \boldsymbol{x}_0(s)$, $\boldsymbol{x}'(\cdot, 0) = \boldsymbol{x}_1(s)$; and boundary conditions $\boldsymbol{x}(0, \cdot) = \boldsymbol{x}_0(0)$, $\boldsymbol{x}(0, \cdot) = \boldsymbol{x}_0(L)$. The second term in (1) is derived from $\Psi := -E(J - 1)^2/2$, the strain energy of a *linearly elastic* material. Furthermore, $J := \|\partial_s \boldsymbol{x}\|$ denotes the determinant of the Jacobian of $\boldsymbol{x}$. The normal $\boldsymbol{n}$ can also be expressed as $\mathcal{R}\partial_s \boldsymbol{x} J^{-1}$ with $\mathcal{R}$ the $\pi/2$ negative rotation. The parameters ϱ_0 and E represent the structural density and Young's modulus respectively. The variational form becomes *find* $\boldsymbol{x} - \boldsymbol{x}_0 \in H_0^1(0, L; \mathbb{R}^2)$ *s.t.* $\forall \boldsymbol{w} \in H_0^1(0, L; \mathbb{R}^2)$*:*

$$(\boldsymbol{w}, \varrho_0 \partial_t^2 \boldsymbol{x})_{L^2} + (\partial_s \boldsymbol{w}, E[1 - J^{-1}]\partial_s \boldsymbol{x})_{L^2} - (\boldsymbol{w}, p\mathcal{R}\partial_s \boldsymbol{x})_{L^2} = 0, \tag{2}$$

with $(\cdot,\cdot)_{L^2}$ the $L^2(0,L;\mathbb{R}^2)$ inner product.

Fluid The Laplace problem with pure Neumann boundaries governs the fluid response, described by ϕ,

$$\begin{cases} \Delta\phi = 0 & \text{in } \Omega, \\ \partial_{\boldsymbol{n}}\phi = g & \text{at } \Gamma, \end{cases} \tag{3}$$

with g the normal velocity at the boundary. These equations can be cast into a boundary integral formulation, as derived in e.g. [8, 12]:

$$c(\boldsymbol{x})\phi(\boldsymbol{x}) + \oint^* H(\boldsymbol{x};\boldsymbol{y})\phi(\boldsymbol{y})d\Gamma_{\boldsymbol{y}} = \oint^* G(\boldsymbol{x};\boldsymbol{y})g(\boldsymbol{y})d\Gamma_{\boldsymbol{y}}, \tag{4}$$

where $\boldsymbol{x} \in \Gamma$ and

$$G(\boldsymbol{x};\boldsymbol{y}) = -(2\pi)^{-1}\log r, \qquad H(\boldsymbol{x};\boldsymbol{y}) = \partial_{\boldsymbol{n}_{\boldsymbol{y}}} G(\boldsymbol{x};\boldsymbol{y}), \tag{5}$$

are the single- and double-layer potentials respectively, with $r := \|\boldsymbol{x}-\boldsymbol{y}\|$ the distance. The coefficient $c(\boldsymbol{x}) = \alpha/2\pi$ with α the local angle of Γ. Recalling our regularity assumptions, $c = 1/2$ a.e. The integrals are singular and, accordingly, the asterisk indicates that these should be interpreted in the *Cauchy principal value* sense. Employing the Galerkin technique, the variational problem corresponding to (4) is: *find* $\phi \in H^{1/2}(\Gamma)$ *s.t.* $\forall w \in H^{1/2}(\Gamma)$*:*

$$(w, \phi/2)_X + (w, H*\phi)_X = (w, G*g)_X\,. \tag{6}$$

The appropriate inner product would be that of $X = H^{1/2}(\Gamma)$ (see [10]), however, the choice $X = L^2(\Gamma)$ is more convenient and is taken as a first attempt.

Coupling The membrane and fluid are coupled kinematically by imposing

$$g = \partial_t \boldsymbol{x}\cdot\boldsymbol{n} \text{ at } \Gamma_w \tag{7}$$

on the fluid and dynamically through the pressure acting on the membrane, by Bernoulli's law,

$$p = \|\nabla\phi\|^2/2. \tag{8}$$

Closure To ensure uniqueness of the coupled problem, two issues are addressed in this paragraph. The first pertains to the nullspace of the Laplace-Neumann equation, the second to a compatibility condition on the boundary data.

It is well-known that (3) is ill-posed, a property that carries over to the boundary integral equation (BIE) (4), see [7]. It follows by substitution that an arbitrary constant can be added to the solution. Thus, the *nullspace* is nontrivial. Physically, the equation is derived to find a velocity field, which is the gradient of ϕ. This constant is therefore

an artifact and it is dealt with by imposing the auxiliary condition $\oint \phi d\Gamma = 0$ through a Lagrange multiplier approach. Accordingly, we add to (6): *find* $\lambda \in \mathbb{R}$ *s.t.* $\forall \mu \in \mathbb{R}$*:*

$$\lambda \oint_\Gamma w d\Gamma + \mu \oint_\Gamma \phi d\Gamma = 0. \tag{9}$$

This freedom in the nullspace comes at the cost of freedom in the choice of valid boundary data, i.e., g has to satisfy a *compatibility condition*. Indeed, by Gauss' theorem, it is apparent that the boundary integral of g should vanish. The boundary data g depends on the structural displacement, however, via the kinematic condition (7), and the structural solution generally does not comply with the compatibility condition. To avoid incompatibility of the structural displacement, a constraint is imposed on the (instantaneous) volume $\mathscr{V}$ of Ω, viz.,

$$C(\boldsymbol{x};t) := \mathscr{V}(\boldsymbol{x}(t)) - \mathscr{V}(\boldsymbol{x}(0)) - \int_0^t \int_{\Gamma_i} v_{\boldsymbol{n}} d\Gamma d\tau = 0. \tag{10}$$

The constraint (10) is again imposed weakly through a Lagrange multiplier approach, by adding to (2): *find* $\lambda \in \mathbb{R}$*, s.t.* $\forall \mu \in \mathbb{R}$*:*

$$\lambda C(\boldsymbol{x};t) + \mu C'(\boldsymbol{x};t)(\boldsymbol{w}) = 0. \tag{11}$$

We remark that (11) is derived from the constrained minimization problem corresponding to (2), see [11].

3 Discretization

Spatial semi-discretization The parametric space $(0, L)$ is partitioned into N_e segments κ^e with maximum length h. This generates the computational mesh $\mathcal{T}_h := \{\kappa^e\}_{e<N_e}$.[1] A $(p+1)$-dimensional polynomial basis $\{N_i(\xi\}_{i\leq p}$ is defined on the reference segment $\hat{\kappa} := (-1, 1)$ and mapped by M^e to each κ^e, such that a solution $\boldsymbol{u} : (0, L) \longrightarrow \mathbb{R}^d$ can be approximated by

$$\boldsymbol{u}(s) \approx \sum_{e,i} N_i \circ [M^e]^{-1} \hat{\boldsymbol{u}}_i^e,$$

where $\hat{\boldsymbol{u}}_i^e \in \mathbb{R}^d$. Following the isoparametric concept, a similar relation holds for the geometry, $\boldsymbol{x}$, of the fluid subproblem. We employ a piecewise linear basis $\{N_i(\xi)\} := \{(1-\xi)/2, (1+\xi)/2\}$. This way, the discrete approximation of Γ satisfies the regularity assumption.

The fluid approximation space is easily derived from that of the structure by reducing the dimension d and appending a discretization of the inflow boundary Γ_i. Where element

[1] Indices i, j and e are taken to run in $\mathbb{N}$ from 0.

integrals are singular, they are evaluated analytically. On the polygonal boundary with linear N_i we find, if $s, s_{\boldsymbol{y}} \in \kappa^e$:

$$(N_i \circ [M^e]^{-1}(s), H(s; s_{\boldsymbol{y}}) * N_j \circ [M^e]^{-1}(s_{\boldsymbol{y}}))_{L^2} = 0,$$
$$(N_i \circ [M^e]^{-1}(s), G(s; s_{\boldsymbol{y}}) * N_j \circ [M^e]^{-1}(s_{\boldsymbol{y}}))_{L^2} = \left(6 + (-1)^{i+j} - 4\log 2J\right) \frac{\boldsymbol{n}_{\boldsymbol{y}} J^2}{8\pi}.$$

Time As elucidated in [5, 3], strong coupling involving an incompressible fluid imposes strong stability requirements on the time discretization. Usually, this entails implicit schemes, such as the 1st-order backward Euler scheme proposed here.[2] The solution vector $\boldsymbol{u}$ of the 2nd-order structural semi-discretization is advanced with time-step τ to time-level $n+1$ by

$$\boldsymbol{M}(\boldsymbol{u}^{n+1} - 2\boldsymbol{u}^n + \boldsymbol{u}^{n-1})\tau^{-2} + \boldsymbol{K}(\boldsymbol{u}^{n+1}) = \boldsymbol{f}^{n+1}, \tag{12}$$

with $\boldsymbol{M}$, $\boldsymbol{K}$ and $\boldsymbol{f}$ the mass, stiffness and forcing derived from (11). A Newton procedure is employed to solve this nonlinear system. Our selection of the Euler scheme is motivated by its simplicity and good numerical damping.

4 Results

Two notes are made on the solution of the discrete system presented in sec. 3. Firstly, to solve the nonlinear weak form of the structure, the Newton procedure is employed. This requires second derivatives of (11) with respect to $\boldsymbol{x}$. The only non-linear term in (2) pertains to the stiffness, and its linearization yields

$$\begin{aligned}\partial_{\boldsymbol{x}} \left[(\partial_s \boldsymbol{w}, J^{-1}\partial_s \boldsymbol{x})_{L^2}\right](\cdot) &= \left(\partial_s \boldsymbol{w}, \frac{\|\partial_s \boldsymbol{x}\|\partial_s(\cdot) - \partial_s \boldsymbol{x}\frac{1}{2}\|\partial_s \boldsymbol{x}\|^{-1}2(\partial_s \boldsymbol{x} \cdot \partial_s(\cdot))}{\|\partial_s \boldsymbol{x}\|^2}\right)_{L^2} \\ &= \left(\partial_s \boldsymbol{w}, [J^{-1}\mathrm{Id} - J^{-3}\partial_s \boldsymbol{x} \otimes \partial_s \boldsymbol{x}]\partial_s(\cdot)\right)_{L^2}\end{aligned}$$

Boundedness of J^{-1} is guaranteed if $\boldsymbol{x}(0,\cdot) \neq \boldsymbol{x}(L,\cdot)$. Note that the tangent stiffness $\partial_{\boldsymbol{x}}(\partial_s \boldsymbol{w}, E[1 - J^{-1}]\partial_s \boldsymbol{x})_{L^2}$ is possibly singular, posing problems for the steady case, such as the hoop stress test presented in this section. In this case the tangent above is approximated by *perfect elasticity* [13], i.e., by letting $J \to \infty$.

Secondly, the volume of the airbag, that is required to impose the compatibility condition 10, can be computed by the determinant rule, according to:

$$\mathscr{V}(\boldsymbol{x}) = \sum_{\mathcal{T}_h} |\hat{\boldsymbol{x}}^e|, \tag{13}$$

where the correct numbering should be noted, i.e., $\forall e < N_e : M^e(-1) < M^e(1)$.

The proposed discretization has been verified by various numerical experiments:

[2] However, recently a 1st-order explicit scheme with defect correction was proposed in [4].

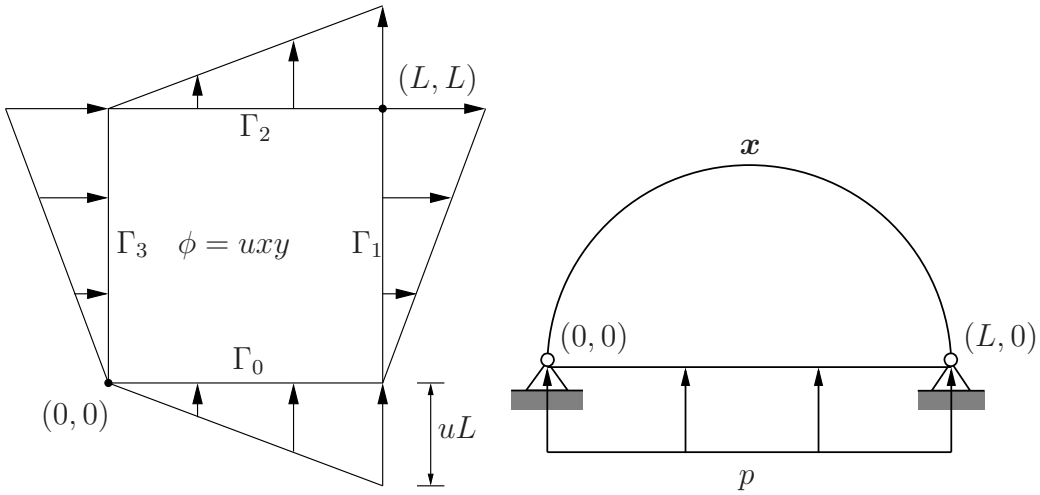

(a) Shearing flow case. (b) Hoop stress case.

Figure 1: Schematics of the test cases.

i) the fluid discretization, by a known solution representing *shearing* motion;

ii) the structural semi-discretization, by finding the *hoop stress*;

iii) the dynamic fluid–structure-interaction formulation, by the inflation of a *pancake*-shaped domain.

Shearing flow To verify the fluid discretization, the solution $\phi = uxy$ is assumed on a unit square. The resulting Neumann conditions suggest the evolution of the boundary from a diamond-shape to a square, see fig. 1a.

The potential and pressure solutions are given in fig. 2. The solution ϕ is very accurate for both quadrature orders. However, in pressure, the tangential derivative clearly reduces the regularity of the solution at the corners of the domain. From the convergence plots in figure 3, we observe the theoretical quadratic convergence [6] in ϕ and the residual, provided quadrature is high enough. If numerical quadrature is used on an element close to the singularity, the quadrature should be sufficiently high. As N_e increases, the neighboring element moves toward this singularity and these errors start to deteriorate the solution, as can be seen from the low-order quadrature curve for p in fig. 3b.

If the inflow is locally perturbed in an incompatible fashion, it can be seen that pressure changes remain local, except increased oscillations at the corners. Thus the pressure distribution does not cause the membrane movement to accommodate the extra inflow, so volume conservation will have to be enforced explicitly, as implied in sec. 2.

Hoop stress To verify the structure discretization, a constant pressure is applied such that a taught string is elongated to a semi-circle. The strain then equals $\pi - 1$, a straight-

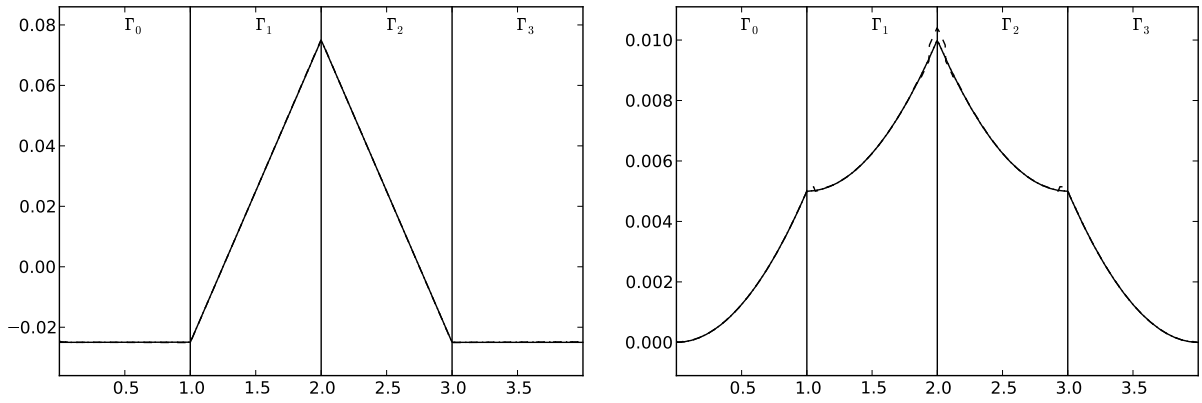

(a) Potential along boundary. (b) Pressure along boundary.

Figure 2: Shearing flow, $N_e = 64$. Plotted are the analytic solution $(-)$, 4^{th}-order $(- -)$ and 32^{nd}-order $(\cdots)$ Gaussian quadrature approximations. Errors of these solutions are given along $(- \cdot -)$ in figure 3b.

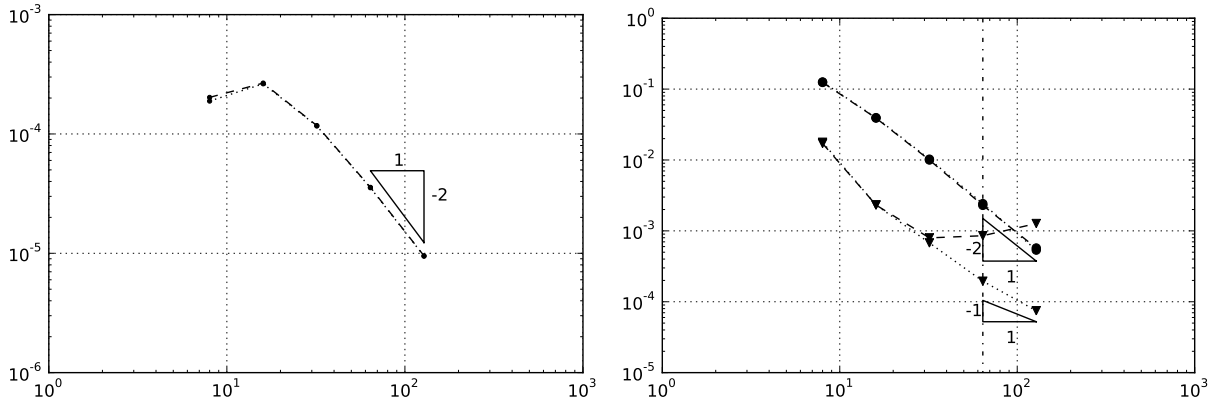

(a) $L^2(\Gamma)$ Riesz representation of the residual. (b) $L^2(\Gamma)$ error norms for ϕ (triangle) and p (circle).

Figure 3: Convergence with N_e (along horizontal axes) for shearing flow w.r.t. the analytical solution of the 4^{th}-order $(- -)$ and 32^{nd}-order $(\cdots)$ Gaussian quadrature approximations.

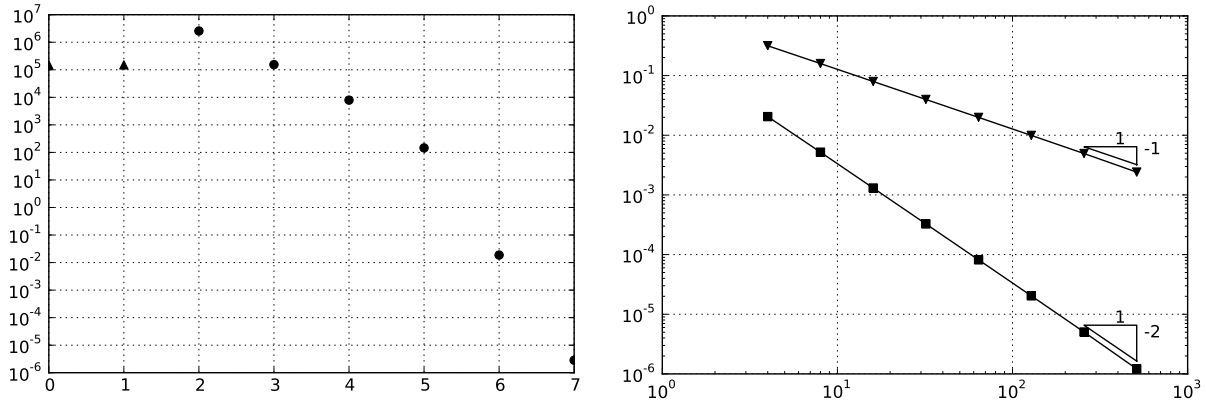

(a) Subiteration residual decay for $N_e = 512$, approximate tangent (triangle), exact tangent (circle).

(b) Spatial convergence (N_e varies along the horizontal axis) w.r.t. the analytical solution, $H^1(0, L; \mathbb{R}^2)$ norm (triangle), $L^2(0, L; \mathbb{R}^2)$ norm (square).

Figure 4: Subiteration- and convergence behavior for the hoop stress case.

forward calculation conveys the required internal pressure $p = (\pi - 2)E/L$, cf. fig. 1b.

We restrict ourselves to the steady, nonlinear problem. In the Newton method, the residual (plotted in fig. 4a) should decay quadratically where the exact tangent is applied, as it is seen to do. Figure 4b shows that the formulation provides linear and quadratic convergence in the H^1 and L^2 norms, respectively. These convergence rates are optimal.

Pancake Finally, we verify the coupled problem qualitatively, by considering a pancake-shaped unstressed initial configuration at rest. An inflow is then applied, following $\partial_t \mathscr{V} = \overline{\partial_t \mathscr{V}} S(s)T(t)$, with

$$S(s) = 4s(L_i - s)/L_i^2$$

$$T(t) = \begin{cases} (1 - \cos(\pi t/T_1))/2, & 0 < t \leq T_1, \\ 1, & T_1 < t \leq T_2, \\ (1 + \cos(\pi(t - T_2)/T_1))/2, & T_2 < t \leq T_1 + T_2, \\ 0, & T_1 + T_2 < t < T. \end{cases}$$

In these relations we have the mean inflation flux $\overline{\partial_t \mathscr{V}} = (\mathscr{V}(0) - \mathscr{V}(T_1 + T_2))/T_2$, inflater opening L_i and two time instances $0 < T_1 \leq T_2$. Note that the mean flux has a negative sign as it is directed into the enclosure. The inflow has a quadratic profile and its magnitude is gradually in- and decreased in time, see fig. 5, which also shows the subiteration history. Snapshots at different time-levels are given in fig. 6. Near the inflater, the membrane is initially concave which causes it to compress under the action of pressure. It is observed that the subsequent wrinkling does not impede the numerical process.

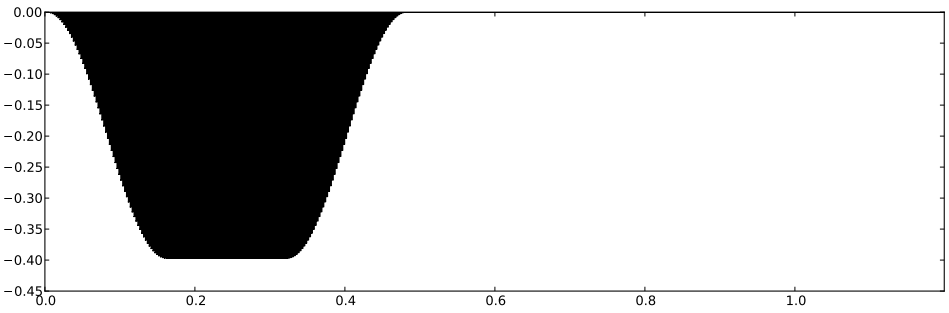

(a) Influx per time-interval.

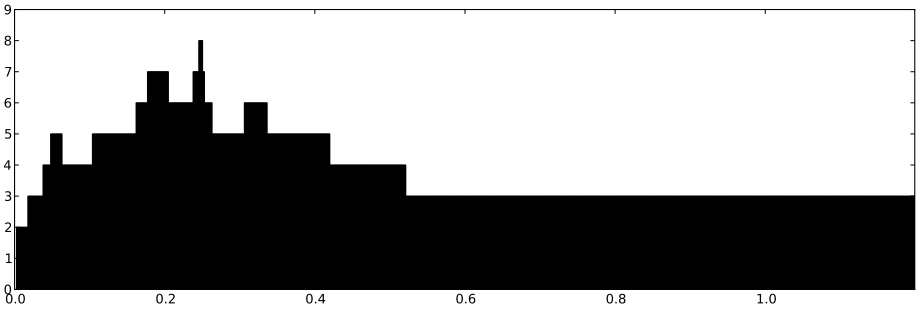

(b) Subiteration count.

Figure 5: Evolution of total inflow (top) and subiteration count (bottom) in time for the pancake test case.

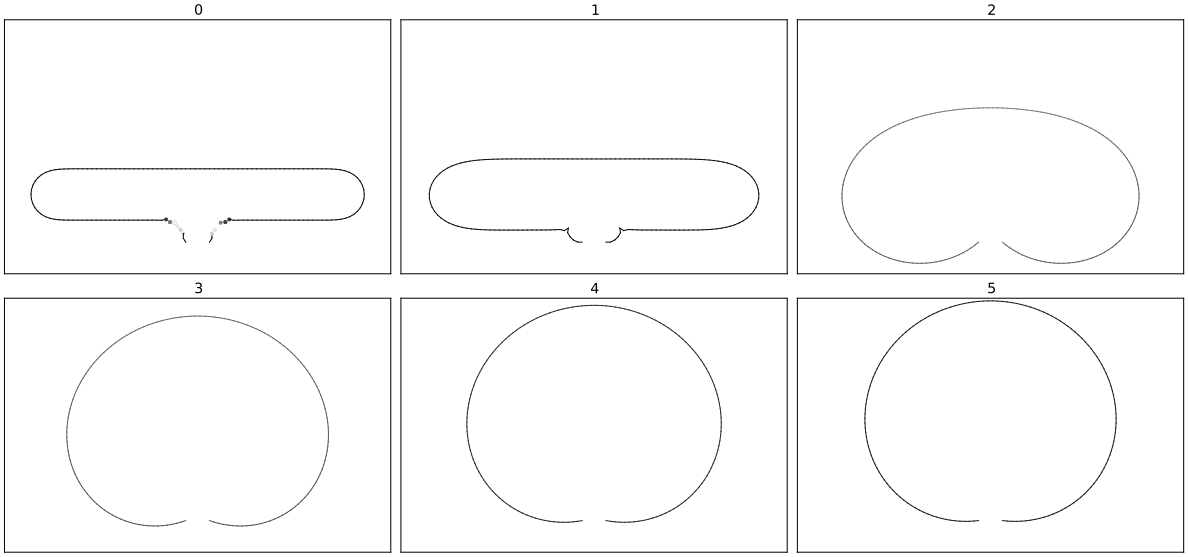

Figure 6: Snapshots of the response in the pancake test case.

5 Conclusions

We have presented an investigation of a computational approach for the simulation of a nonlinear membrane in interaction with an inviscid, incompressible and irrotational fluid, based on the boundary element method. We showed that the compatibility condition on the boundary velocity originating from the incompressibility of the fluid, must be imposed explicitly on the structural motion as an auxiliary constraint. Numerical experiments conveyed optimal convergence of the finite-element approximations of the fluid and structure subsystems, and of the coupled fluid-structure-interaction problem. Our results indicate that BEM provides a very effective approach to large-displacement fluid-structure interactions on geometrically complex domains, because it avoids the mesh degradation inherent to standard volumetric discretization methods. Moreover, it significantly reduces the computational complexity, because the fluid solution is only computed on the boundary.

REFERENCES

[1] Stuart S. Antman. The equations for large vibrations of strings. *The American Mathematical Monthly*, 87(5):359–370, 1980.

[2] E. H. Brummelen, van. Partitioned iterative solution methods for fluid–structure interaction. *International Journal for Numerical Methods in Fluids*, 65(13):3–27, 2002.

[3] E. H. Brummelen, van. Added mass effects of compressible and incompressible flows in fluid-structure interaction. *Journal of Applied Mechanics*, 76(2), 2009.

[4] Erik Burman and Miguel A. Fernández. Stabilization of explicit coupling in fluid-structure interaction involving fluid incompressibility. *Computer Methods in Applied Mechanics and Engineering*, 198(5-8):766–784, 2009.

[5] P. Causin, J. F. Gerbeau, and F. Nobile. Added-mass effect in the design of partitioned algorithms for fluid-structure problems. *Computer Methods in Applied Mechanics and Engineering*, 194(42-44):4506–4527, 2005.

[6] W. Dijkstra, G. Kakuba, and R.M.M. Mattheij. Condition numbers and local errors in the boundary element method. Technical report, Eindhoven, University of Technology, P.O. Box 513, 5600MB, Eindhoven, Netherlands, 2008.

[7] W. Dijkstra and R.M.M. Mattheij. A relation between the logarithmic capacity and the condition number of the bem-matrices. *Communications in Numerical Methods in Engineering*, 23:665–680, 2007.

[8] S. Liapis. An adaptive boundary element method for the solution of potential flow problems. *Engineering Analysis with Boundary Elements*, 18:29–37, 1996.

[9] P.-O. Marklund and L. Nilsson. Simulation of airbag inflation processes using a coupled fluid structure approach. *Computational Mechanics*, 29(4-5):289–297, 2002.

[10] W. McLean. *Strongly elliptic systems and boundary integral equations*. Cambridge University Press, 2000.

[11] Brian Moran Ted Belytschko, Wing Kam Liu. *Nonlinear Finite Elements for Continua and Structures*. Wiley, 2000.

[12] L.C. Wrobel. *The Boundary Element Method*, volume 1. Applications in Thermo-Fluids and Acoustics. John Wiley & Sons, 2002.

[13] D. Yong. Strings, chains and ropes. *SIAM*, 48(4):771–781, 2006.